Published in Clay Minerals 36, 171-180, 2001, which should be used for any reference to this work

Finite strain has no influence on the illite crystallinity of tectonized Eocene limestone breccias of the Morcles nappe, Swiss Alps

M. BURKHARD* AND N. BADERTSCHER

Institut de Géologie, Université de Neuchâtel, rue E. Argand 11, CH 2007 Neuchâtel, Switzerland

ABSTRACT: The relationship between illite crystallinity (IC) and finite strain as well as lattice strain and crystallite size of illite is examined in a series of 27 deformed breccia samples from the inverted limb of the Morcles nappe. The IC is determined independently for limestone components and a red/green clay-silt matrix. The finite strain varies widely (D = 0.8−2.5). The IC values vary from diagenetic to epizonal, but no correlation with finite strain could be established. The spread of IC values is explained by heterogeneities within the protolith which have not been homogenized/ obliterated by the anchi- to epizonal metamorphic overprint. While limestone pebbles display IC values in agreement with the regional metamorphic conditions, the clay-silt matrix has anomalously high IC values, even after deconvolution of the 10 Å peak to correct for the presence of paragonite/ muscovite. No correlation could be established between finite strain, lattice strain and/or crystallite size of illite.

KEYWORDS: strain, illite crystallinity, limestone breccias, Morcles nappe, Switzerland.

This paper was presented at a colloquium held at the University of Lausanne on 20th May 1999 in honour of Professor Bernard Kübler, who subsequently died on 16th September 2000

Illite crystallinity (IC) measurements are a convenient and quick way to characterize the degree of very low to low grade metamorphism in sedimentary series (Frey, 1987; Frey & Robinson, 1999). Unfortunately, however, the time-temperature paths of burial are not the only factor influencing IC. Locally variable conditions, especially the compositions of the protoliths, probably aided by variations in fluid circulation, fluid chemistry, deformation intensity and many more variables influence the final clay mineral assemblage (Kisch, 1990; Roberts *et al*., 1991; Arkai *et al*., 1997). The IC measurements therefore never quite succeeded in reaching the status of a reliable absolute 'palaeothermometer' neither in basin or in metamorphic petrological studies.

Tectonic strain has often been postulated as a potential factor influencing IC. In theory, deformation could act in two different ways to either increase or decrease crystallinity. Intracrystalline deformation of the illite crystals at low temperature is expected to lead to an accumulation of elastic distortion, accumulation of lattice defects, and reduction in the size of grains, subgrains and crystallites. Corresponding X-ray line broadening, a well known effect from cold work in metals (Warren & Averbach, 1950), leads to a increase in IC. On the other hand, deformation-enhanced syntectonic recrystallization of illite and detrital muscovite could produce a large population of

* E-mail: martin.burkhard@unine.ch

strain-free 'new' and larger grains with excellent ('low value') crystallinities. The relative importance of the two processes, deformation and recovery, is strongly dependent on temperature, strain rate and/or differential stress during deformation/recrystallization (Urai *et al*., 1986). Apart from this direct influence on IC, deformation processes may also have an indirect influence on IC through deformation-enhanced permeability and fluid advection (McCaig & Knipe, 1990). Fluid circulation along localized shear zones may favour the formation of newly crystallized hydrothermal illites with potentially excellent crystallinities.

Previous field studies had limited success in documenting a direct influence of finite strain on IC (Flehmig, 1973; Flehmig & Langheinrich, 1974; Nyk, 1985). Most of these studies involved folds or shear zones and detected only slight changes in IC which were independent of position within these structures. Arkai *et al*. (1997) compared IC, mean lattice strain and mean crystallite size of illite and chlorite across the Glarus thrust. In this example, the tectonic strain effect on crystallite size (decreasing) and lattice strain (increasing) seem to cancel each other out in terms of IC ($\pm$ constant) (Fig. 1−4 in Arkai *et al*., 1997). Finite strain, however, has not been measured in any of theses studies.

In this paper we test the influence of finite strain intensity on IC in a quantitative way. A wide range of finite strain intensities is observed in the lower Helvetic Morcles nappe of western Switzerland. At the nappe scale (15 km NW−SE), the frontal and upper parts of the nappe are very weakly deformed despite km-scale tight folding, whereas extremely high strains are encountered within the inverted limb and at the rear of the nappe, the so called 'helvetic root zone'. Very strong strain gradients also occur on a much smaller (100 m) scale, most notably within individual folds of the inverted limb. A variety of finite strain markers has been described and studied extensively in the Morcles nappe (Siddans, 1971; Ramsay & Huber, 1983; Ramsay & Huber, 1987). We have chosen a conspicuous breccia horizon at the top of the Cretaceous limestone series which allows for a macroscopic determination of finite strain using classic R_f/ϕ techniques. This breccia is composed of cm- to dm-sized angular Middle Cretaceous limestone fragments embedded in a red or green silty clay matrix. This matrix is interpreted as a reworked lateritic palaeosoil of probable Eocene age (Mayoraz, 1995). Similar, Fe-rich material is found in palaeokarst pockets at the top of the Mesozoic series, marking the foreland unconformity between Mesozoic passive margin series in the footwall and a Neogene clastic wedge in the hangingwall (Burkhard & Sommaruga, 1998). The IC of both matrix and limestone components were analysed and compared with each other and *vs*. the measured strain intensities. Samples were collected from metre-sized boulders in a rock fall which must have occurred shortly after the last glacial maximum on the south side of the Dt. du Midi (Fig. 1). The angular shape and the freshness of the fracture surfaces of a large number of boulders make them ideal for 3-D strain analyses. Finite strain determinations were made on three to four different (2-D) faces of each boulder (Fig. 2). Our samples were not oriented with respect to the Morcles nappe, nor can we identify the precise provenance of each sample within the fold structure. However, the provenance of these boulders is restricted to the SW side of the Pointe de la Gagnérie mountain, an area of <500 by 200 m (Gagnebin, 1934). The breccia boulders stem from a single thin stratigraphic horizon (De Loys, 1928) and we are therefore confident that all samples have been exposed to an identical time-temperature evolution during deformation of the Morcles nappe.

In summary, our sampling strategy provides limestone samples of limited lithologic variety, mostly Lower Cretaceous carbonate pebbles, which were assembled during Eocene extensional tectonics in a fault scarp breccia and embedded in an Fe-rich silty clay matrix. During alpine deformation, this breccia horizon was folded concordantly together with footwall Cretaceous limestones and deformed to variable degrees of finite strain within an isoclinal fold of the inverted limb of the Morlces nappe.

SAMPLING AND ANALYTICAL TECHNIQUES

Sampling and strain measurements

The aspect ratio of breccia components seen on different boulder faces varies from near circular to highly elongate (Fig. 2) as a function of both strain intensity and cut effects. In order to quantify finite strain in three dimensions, we selected boulders according to the following criteria: (1) there was good optical contrast between light breccia

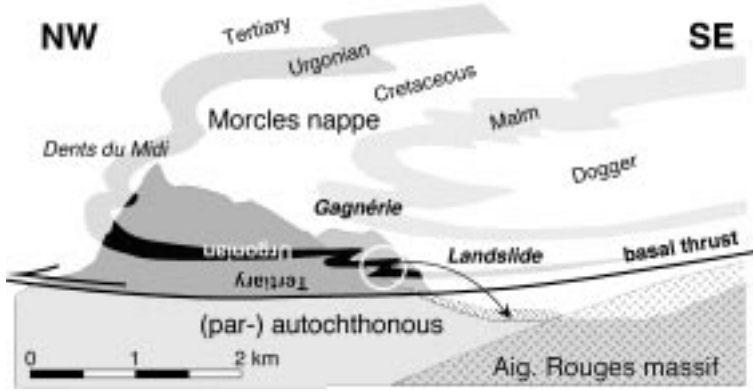

FIG. 1. Cross-section of the Morcles nappe in the Dt. du Midi area. A landslide on the western side of the Gagnérie mountain includes variably deformed Eocene breccias from an isoclinal fold structure in the inverted limb of the nappe.

components and the coloured matrix; (2) there were at least three accessible flat faces at high (close to 90°) angles between each other; and (3) there were at least 10, and ideally more than 30 pebbles visible on each face of the boulder. Each boulder face was marked with a reference circle of known dimension, geographic orientation markers (azimuth and dip), numbered and photographed. The shapes of the components were hand-drawn from enlarged colour photographs. Line drawings were scanned and corrected for slight photographic distortions by restoring the reference circle. Image 3.1 software (NCSA, 1997) was used for automatic recording of the following data for each pebble: longest diameter, shortest diameter, orientation of longest diameter, surface area, perimeter and centre coordinates. Strain analyses were performed in an Excel worksheet according to the Matrix method (Shimamoto & Ikeda, 1976) and the Polar method (Elliott, 1970). In all cases, both methods yield very similar results to within <5% of each other.

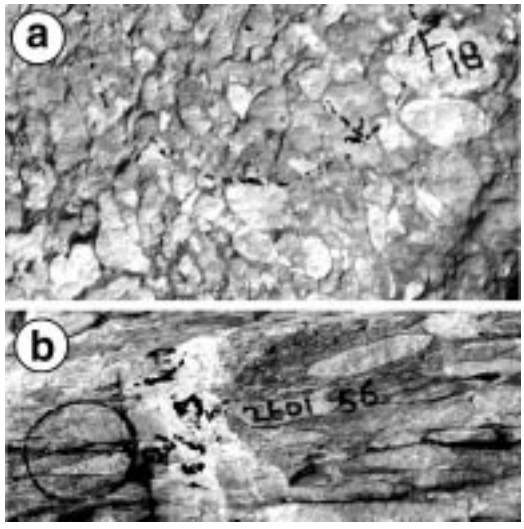

FIG. 2. Two field photographs of breccia samples (horizontal width ~30 cm) in which light coloured Lower Cretaceous limestone fragments are embedded in a silty clay matrix. The black circle and arrows were used for orientation purposes. (a) Weakly deformed sample F18 with a finite strain of D = 0.87. (b) Strongly deformed sample F16 with finite strain of D = 1.96. For the significance of the D value, see Fig. 3.

The 3-D strains were calculated from the three (or four) 2-D faces using TRISEC (Milton, 1980), TRXL (Gendzwill & Stauffer, 1981) and/or PASE5 (Siddans, 1971). The 3-D strains are overdetermined with three or more 2-D sections through the strain ellipsoid, which is handled in different ways by each technique. In order to test the 3-D results, we systematically cut the best-fit 3-D ellipsoids along the original 2-D boulder face orientations using ELLIPSE (Gendzwill & Stauffer, 1981). We thus compared misfits between observed and calculated finite strains for each face and the various techniques applied. In cases where TRXL and TRISEC results gave significantly different 3-D

strains, we retained the result with the more conservative calculated strain value for the 2-D face with the highest measured R_f axial ratio (Table 1). From the retained 3-D strain values, we calculated the *D* value (Ramsay & Huber, 1983) for the finite strain intensity of each boulder. This *D* value corresponds to the absolute distance between the origin and a strain value plotted on a logarithmic Flinn diagram (Fig. 3). This *D* value was used for a comparison of finite strain intensity with IC.

Samples were taken from each boulder for X-ray diffraction (XRD) analysis. Whenever possible, limestone pebbles and clayey-silt matrix were sampled separately for a clay mineral charaterization. In a few cases of component-supported breccias, we were unable to obtain a pure 'matrix' sample. These are listed as 'pebbles and matrix mixture' in Table 1.

Illite cystallinity measurements

The IC values (Kübler, 1964, 1967) were determined from oriented clay mounts prepared according to standard techniques used at Neuchâtel. For sample preparation and instrumental XRD settings, see Burkhard & Goy-Eggenberger (2001). Measurements were made for the <2 μm and 2−16 μm grain size-fractions, both air dried and glycolated, thus leading to four different IC values per sample. The presence of variable amounts of mixed-layer minerals rectorite and/or muscovite-paragonite in many of the analysed samples leads to an anomalous broadening of the 10 Å peak. While such samples are simply discarded in regional IC studies, we chose to correct systematically for this influence by applying a peak decomposition of the 10 Å reflection using a fast Fourier transformation (included in the Scintag analysis software package). The 'full width at half maximum' (FWHM) of the deconvoluted 10 Å peak is systematically smaller than the raw one; absolute values thus obtained cannot be compared to regional metamorphism studies unless a similar transformation is applied to the IC standards. In order to avoid the superposition of peaks from different phases, we also measured the raw and deconvoluted crystallinity of the illite 005 peak, whenever it was >250 cps high. Unfortunately, only about half of the samples met this criterion, but they confirmed the reliability of the deconvolution procedure to obtain a 'pure' 10 Å illite peak.

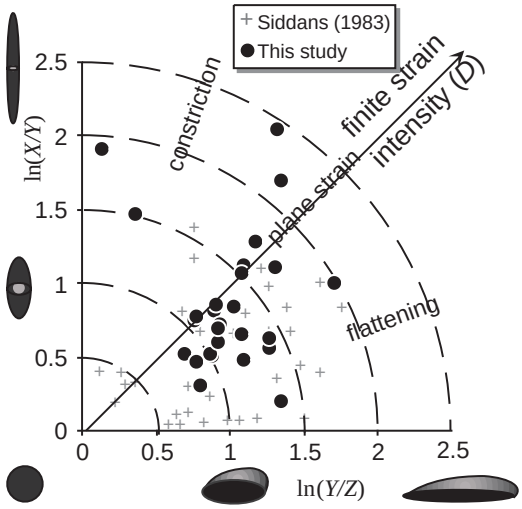

FIG. 3. Logarithmic Flinn diagram, illustrating the results of all finite strain determinations. The values *X, Y* and *Z* represent the longest, intermediate and shortest axes of the 3-D strain ellipsoid, respectively. The parameter *D*, equal to the distance from the origin, is a convenient means of characterizing the finite strain intensity irrespective of the shape of the strain ellipsoid.

RESULTS

Twenty seven samples were examined for both 3-D finite strain and clay mineral characteritics. The results are summarized in Table 1.

Finite strain

The 3-D strain results are represented in a Flinn-diagram (Ramsay & Huber, 1983), or rather its logarithmic form, also called 'Ramsay-diagram', shown in Fig. 3. While the majority of samples fall in the flattening field ('pancakes'; $X>Y>1$, $Z<1$), there are a few notable exceptions of markedly constrictional ellipsoids (cigar shapes; $X>1$, $Z<Y<1$). The finite strain intensities *D* vary considerably, from 0.86 to 2.45. This corresponds to a range of 2.5−7.5 for axial ratios ($R_{max} = X/Z$ for equivalent plane strain ellipsoids). Note that the largest measured axial ratio on any boulder face (listed as R_{max} measured in Table 1) is not a very good way of characterizing the intensity of the 3-D finite strain, because 2-D axial ratios are strongly

TABLE 1. IC values of the air-dried <2 μm clay fraction, compared to finite strain values.

Sample #	Illite crystallinity (10 Å peak) IC	deconvoluted 10 Å peak				Finite strain from pebbles R_{max}	3-D finite strain parameters			
Matrix:	meas.	IC dec.	cps.	Area	β	measured	k	d	D	Method
F2	0.530	0.400	1118	29175	0.435	3.72	0.30	1.27	0.86	TRXL
F3	0.352	0.295	1035	21507	0.346	3.64	0.47	1.56	1.02	TRXL
F4	0.420	0.330	1083	25529	0.393	4.87	0.34	2.67	1.41	Trisec
F5	0.464	0.378	381	10240	0.448	8.26	0.76	3.35	1.71	Trisec
F6	0.331	0.224	487	8079	0.276	4.26	0.88	1.89	1.20	Trisec
F7	0.620	0.449	598	18077	0.504	3.85	7.48	3.35	1.51	TRXL
F8	0.463	0.378	1822	48136	0.440	4.95	0.49	2.12	1.25	TRXL
F9	0.499	0.409	773	22400	0.483	2.89	1.00	1.56	1.05	TRXL
F11	0.331	0.280	1096	22809	0.347	7.01	0.49	1.53	1.01	TRXL
F13	0.435	0.368	1461	35980	0.410	3.55	0.74	2.21	1.32	Trisec
F15	0.368	0.271	327	5836	0.297	5.77	1.04	2.86	1.57	TRXL
F16	0.370	0.322	1039	23545	0.378	4.12	0.40	4.70	1.96	TRXL
F17	0.434	0.342	883	21009	0.397	3.77	0.54	1.72	1.10	Trisec
F19	0.274	0.256	1177	21477	0.304	5.53	1.16	3.46	1.75	Trisec
F20	0.360	0.333	594	15095	0.424	5.86	0.29	2.69	1.39	Trisec
F22	0.597	0.435	948	27543	0.484	4.68	0.08	2.89	1.37	Trisec
F25	0.420	0.419	112	3543	0.527	3.5	0.98	1.68	1.11	TRXL
F27	0.317	0.251	1225	21844	0.297	5.51	0.70	1.86	1.18	Trisec
F28	0.295	0.256	2134	40810	0.319	4.03	0.93	1.98	1.24	Trisec
Average	0.415	0.337	±0.07							
Pebbles										
F2	0.313	0.282	1796	39482	0.366	3.72	0.30	1.27	0.86	TRXL
F3	0.251	0.207	407	6876	0.282	3.64	0.47	1.56	1.02	TRXL
F4	0.412	0.364	2203	58230	0.441	4.87	0.34	2.67	1.41	Trisec
F5	0.493	0.402	1472	39749	0.450	8.26	0.76	3.35	1.71	Trisec
F6	0.316	0.210	680	10391	0.255	4.26	0.88	1.89	1.20	Trisec
F7	0.302	0.238	482	8214	0.284	3.85	7.48	3.35	1.51	TRXL
F8	0.324	0.321	1389	31458	0.377	4.95	0.49	2.12	1.25	TRXL
F9	0.309	0.268	1262	25218	0.333	2.89	1.00	1.56	1.05	TRXL
F11	0.324	0.305	968	21088	0.363	7.01	0.49	1.53	1.01	TRXL
F13	0.177	0.180	362	5337	0.246	3.55	0.74	2.21	1.32	Trisec
F15	0.339	0.264	1093	19992	0.305	5.77	1.04	2.86	1.57	TRXL
F16	0.224	0.204	684	11614	0.283	4.12	0.40	4.70	1.96	TRXL
F17	0.294	0.270	843	16540	0.327	3.77	0.54	1.72	1.10	Trisec
F19	0.258	0.246	1376	23188	0.281	5.53	1.16	3.46	1.75	Trisec
F20	0.229	0.192	925	14022	0.253	5.86	0.29	2.69	1.39	Trisec
F22	0.376	0.295	992	22789	0.383	4.68	0.08	2.89	1.37	Trisec
F25	0.446	0.302	819	20477	0.417	3.5	0.98	1.68	1.11	TRXL
F27	0.302	0.158	1157	13079	0.188	5.51	0.70	1.86	1.18	Trisec
F28	0.361	0.210	601	8714	0.242	4.03	0.93	1.98	1.24	Trisec
Average	0.318	0.259	±0.06							
Pebbles and matrix mixture:										
F1	0.369	0.369	2621	66649	0.424	4.15	1.02	2.72	1.52	TRXL
F4	0.361	0.396	1813	50142	0.461	4.87	0.34	2.67	1.41	Trisec
F10	0.346	0.267	2494	45775	0.306	8.48	41.14	5.76	1.91	TRXL
F14	0.383	0.402	852	23095	0.452	4.62	0.65	1.81	1.15	Trisec
F18	0.318	0.289	1206	26235	0.363	3.62	0.66	1.23	0.87	TRXL
F21	0.162	0.133	718	5927	0.138	7.39	1.57	5.33	2.18	Trisec
F23	0.441	0.353	2357	61623	0.436	3.91	0.32	2.06	1.19	TRXL
F24	0.391	0.412	728	19710	0.451	2.82	0.50	1.32	0.91	TRXL
F26	0.413	0.327	1320	31927	0.403	6.2	2.34	7.31	2.45	TRXL

R_{max}: largest measured strain ratio on 2-D boulder face
IC: Illite (10 Å) crystallinity, air dry
IC dec: deconvoluted IC
cps: counts per second (10 Å peak)
area: area below 10 Å peak
β: integral breadth (area/peak height)
k: $(R_{xy} - 1)/(R_{yz} - 1)$
d: $((R_{xy} - 1)^2 + (R_{yz} - 1)^2)^{0.5}$
D: $((E_1 - E_2)^2 + (E_2 - E_3)^2)^{0.5}$, where $E_x = \ln(1 + e_x)$
TRXL: Gendzwill & Stauffer (1981)
Trisec: Milton (1980)

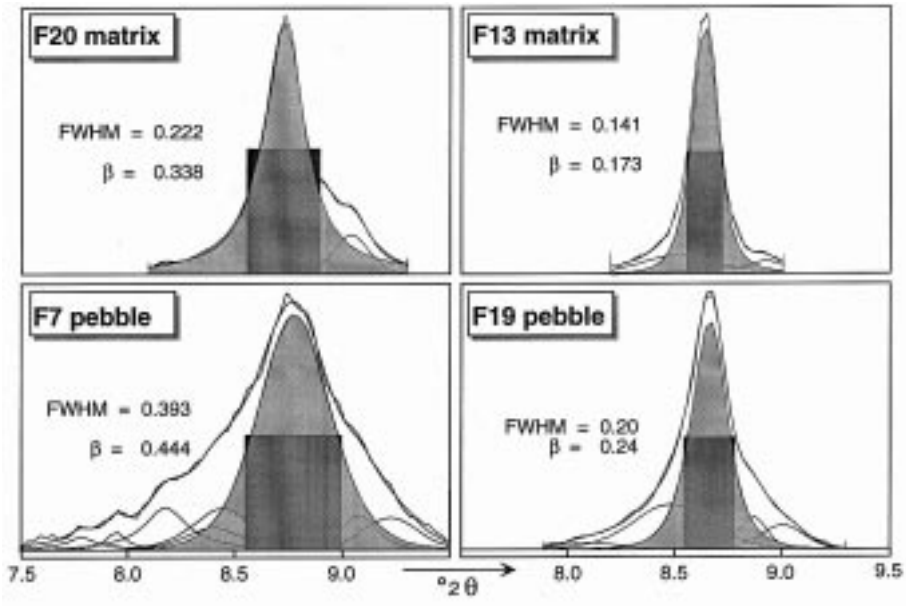

FIG. 4. Representative XRD patterns of the glycolated illite (10 Å) peak, from the <2 μm clay fraction. The net intensities after background removal and $K\alpha_2$ stripping are deconvoluted. The deconvoluted illite peak is shaded in grey. Note the large variations in IC (FWHM) encountered in pebbles and in the matrix samples. The integral breadth (β) is visualized through the use of a rectangular black box with half of the area and half of the height of the peak and put behind the semi-transparent illite peak.

dependent on cut effects of the boulder faces with respect to the orientation of the strain ellipsoid.

For comparison (Fig. 3), we superimposed a population of finite strains measured elsewhere in the Morles nappe (Siddans, 1983). It is interesting to note that strain variations recorded on the scale of the nappe are in the same range as those encountered in a single fold of the inverted limb.

Clay mineralogy, illite crystallinity

The XRD analysis of 19 matrix samples revealed the presence of an abundance of clay minerals (>40%), followed by calcite (25%), quartz (silt fraction) (25%) and traces of albite. The clay mineral separates were dominated by about equal amounts of chlorite and illite plus variable quantities of mixed-layer minerals rectorite and/or muscovite-paragonite. The latter were in part responsible for a large spread in IC values, ranging from 0.27 to 0.62°2θ (<2 μm, glycolated). This spread was significantly reduced when the FWHM of the deconvoluted 10 Å peak was considered.

The IC values ranged from 0.18 to 0.49 for the raw, and from 0.16 to 0.4°2θ for the deconvoluted illite peak. The average deconvoluted IC ($0.337°2\theta \pm 0.07$, σ) put the matrix in the field of diagenesis.

Pebbles analysed from the same 19 boulders were invariably pure limestone, with >95% calcite. The insoluble residues were dominated by illite, chlorite and traces of quartz and albite. The latter two were absent from the <2 μm grain size-fraction. The presence of mixed-layer minerals was more pronounced in clay-silt matrix than in the carbonate pebbles. With values ranging from 0.22 to 0.45°2θ FWHM, however, the IC values were still far from homogeneous. On average, deconvoluted IC values (0.259 ± 0.06, 1σ) indicated a very low-grade metamorphism within the anchizone (0.33 to 0.22°2θ, in agreement with the metamorphic zonation established on the regional scale (Burkhard, 1988).

Lattice strain and apparent crystallite size of illite

The deconvoluted peak shape of the 10 Å illite peak has also been used to infer lattice strain and

mean apparent crystallite size using the Voigt function (De Keijser *et al*., 1982). This approach is similar to the one followed and discussed in detail by Arkai *et al*. (1996, 1997). A visual inspection of various deconvoluted illite peaks showed some striking variations not only in IC but also in the peak shapes. These differences are highlighted in Fig. 4, where the integral breadth is visualized using a rectangle of half of the area and half of the height of the 10 Å peak. As an 'undeformed' illite standard for comparison and Voigt-calculations, we used a greenschist-facies Cretaceous limestone sample from the rear of the Doldenhorn nappe (Burkhard, 1988) with an IC of 0.14 and an integral breath of 0.16°2θ. While this sample is not tectonically undeformed by any means, it clearly has undergone a greater degree of metamorphism and is recrystallized to a fine-grained marble. From theoretical restrictions of the method it is obvious that neither lattice strain (expressed in dimensionless ratio or percent) nor apparent crystallite size (in Å) can be regarded as absolute values.

The results (Fig. 5) show that there was a considerable spread in both lattice strain and crystallite size. Apparent lattice strain varied from 0 to 0.1 with a mean value of 0.05 ± 0.02, while the apparent crystallite size varied from 380 to 6500 Å with a mean value of 1267 ± 1069 Å. Graphically (Fig. 5), there seems to be a vague positive correlation between lattice strain and size. Statistically, however, this correlation is not significant with R^2 of only 0.009. No recorrelation between lattice and finite strain could be established either.

DISCUSSION AND CONCLUSION

IC vs. finite strain

The comparison of finite strain with IC values shows no correlation at all (Fig. 6). Linear regression lines seem to indicate a slight tendency for increasing IC values with increasing strain both in matrix and pebbles. Correlation coefficients, R^2, of 0.023 and 0.077 disprove any such trend,

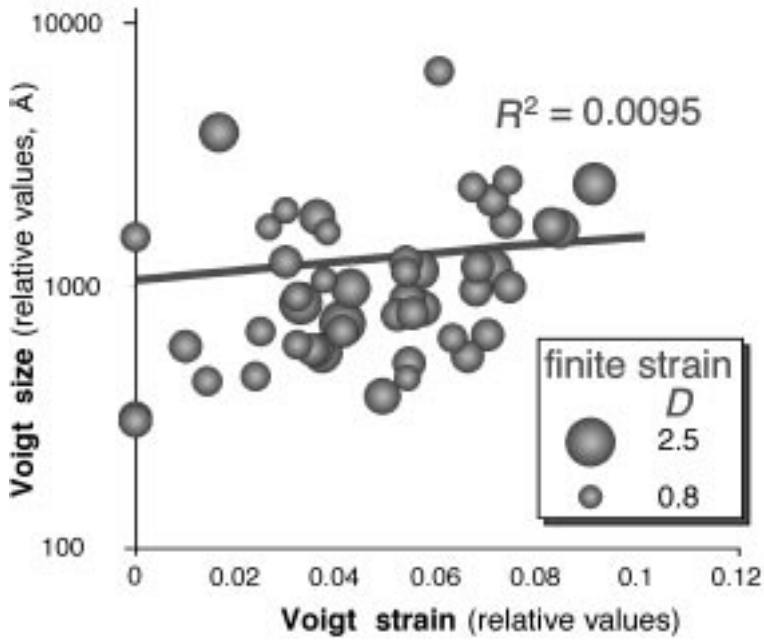

FIG. 5. Crystallite size plotted against apparent lattice strain. Both parameters are determined using the Voigt function (according to a procedure by DeKeijser *et al*., 1982). An apparent weak correlation between these two parameters (grey line) is not significant (R^2 = 0.0095). Finite strain (D) is visualized through the size of the circles; vertical stacking order is from highest finite strain to lowest (at the top). No correlation exists between finite and lattice strain.

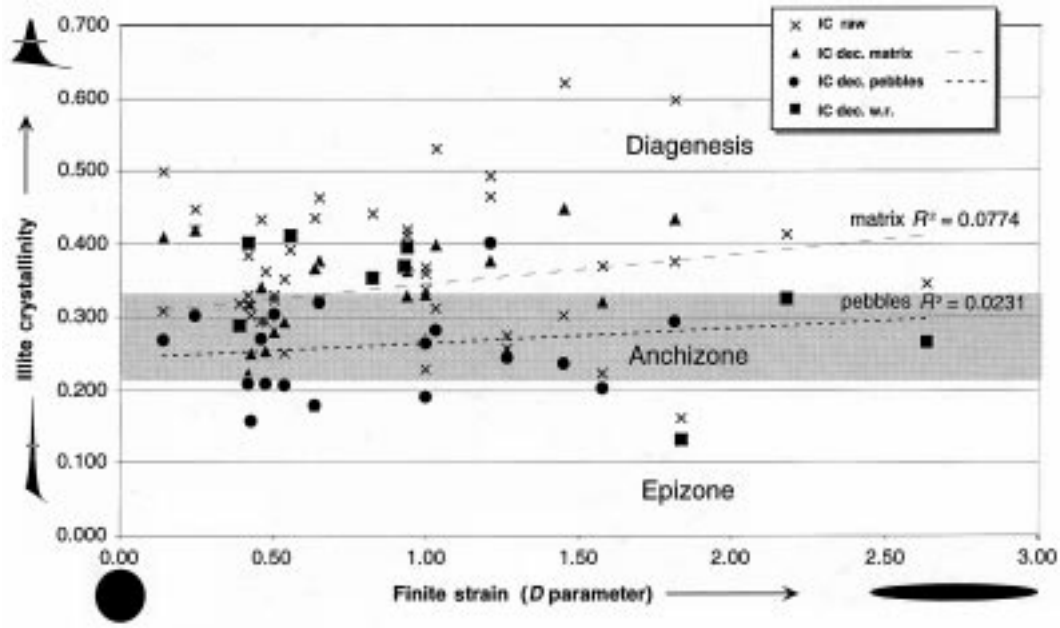

FIG. 6. Illite crystallinity (<2 μm, glycolated) plotted against finite strain. No correlation exists between these two parameters – as indicated by linear regression lines and corresponding R^2 values for matrix and pebbles.

however. Instead, a large scatter of IC values was observed over the entire range of deformation intensities. The deconvolution procedure, intended to remove the effect of variable amounts of mixed-layer minerals in the samples, did not significantly reduce this scatter. This observation, made within boulders of the Gagnérie landslide, is in agreement with observations made on the scale of the Morcles nappe (Burkhard & Goy-Eggenberger, 2001) and elsewhere in the Helvetic zone (Burkhard, 1988). Illite crystallinity values did show a large scatter among individual samples from a single sampling site and even within individual stratigraphic horizons. This scatter has to be attributed to subtle variations in protolith composition rather than differences in the time-temperature evolution (identical in all samples). We were unable to find any relationship between finite strain and IC in strongly-deformed Eocene breccias from the inverted limb of the Morcles nappe. If any such influence existed, it would be completely obscured by the heterogeneity existing among different protoliths – in our case, various Cretaceous limestones and an Eocene clayey-silt matrix.

Lithology bias

In a companion study, Burkhard & Goy-Eggengerger (2001) we were able to demonstrate that variable calcite content (shale, marl, limestone) does not have any systematic influence on the average IC within sampling profiles nor on the scale of the entire Morcles nappe. Goy-Eggenberger (1998) could not find any other lithology bias within 268 samples from the Morcles nappe. The present study of Eocene breccias, led to a different conclusion, however. Two anomalies were detected within the Eocene breccia samples of the Gagnérie mountain. First of all, the average 'raw' IC values measured in this study fell within the diagenesis range while the regional metamorphic grade of this area is close to the anchizone-epizone boundary (for a compilation of data, mostly from unpublished Neuchâtel diploma theses, see Burkhard, 1988). This discrepancy is at least in part explained by the presence of minor amounts of mixed-layer illite-smectite and paragonite-muscovite. Normally, such samples would have been discarded from a regional metamorphism study. In order to compensate for

this influence, we chose to systematically apply a peak deconvolution procedure. Even the deconvoluted IC values, however, were still rather large . A second anomaly was observed in the comparison of limestone pebbles and their silty clay matrix. With a population of 19 samples, the observed difference of 0.078 in the average IC values between pebbles ($0.259^\circ 2\theta \pm 0.06$) and matrix ($0.337 \pm 0.07$) was significant. This, therefore, demonstrated a lithology bias in the IC values. Based on the expected metamorphic grade of the area, the IC of the clay-silt matrix seems to be too low, while IC values of the pebbles more closely reflect an anchizonal regional metamorphic grade. We do not have independent proof for this statement, however.

Lattice vs. finite strain and crystallite size

No correlation could be found between lattice strain, crystallite size and finite strain (Fig. 5).

In summary, we conclude that the initial heterogeneity among seemingly quite similar limestones and between their red-green clay-silt matrix are the main reasons for the large spread of observed IC values. Alpine metamorphic overprint of an estimated anchizonal degree has not succeeded in obliterating/homogenizing such heterogeneities. Finite strain intensity does not correlate with illite crystallinity, lattice strain or crystallite size as determined from the deconvoluted 10 Å peak.

REFERENCES

Arkai P., Merriman R.J., Roberts B., Peacor D.R. & Toth M. (1996) Crystallinity, crystallite size and lattice strain of illite-muscovite and chlorite; comparison of XRD and TEM data for diagenetic to epizonal pelites. *Eur. J. Mineral.* **8**, 1119–1137.

Arkai P., Balogh K. & Frey M. (1997) The effects of tectonic strain on crystallinity, apparent mean crystallite size and lattice strain of phyllosilicates in low-temperature metamorphic rocks. A case study from the Glarus overthrust, Switzerland. *Schweiz. Mineral. Petrogr. Mitt.* **77**, 27–40.

Burkhard M. (1988) L'Helvétique de la bordure occidentale du massif de l'Aar (évolution tectonique et métamorphique). *Eclog. Geol. Helv.* **81**, 63–114.

Burkhard M. & Goy-Eggenberger D. (2001) Near vertical iso-illite-crystallinity surfaces cross-cut the recumbent fold structure of the Morcles nappe, Swiss Alps. *Clay Miner.* **36**, 157–168.

Burkhard M. & Sommaruga A. (1998) Evolution of the western Swiss Molasse basin: structural relations with the Alps and the Jura belt. Pp. 279–298 in: *Cenozoic Foreland Basins of Western Europe* (A. Mascle, C. Puigdefàbregas, H.P. Luterbacher & M. Fernàndez, editor). Spec. Publ. **134**. Geological Society, London.

De Keijser H., Langford J.I., Mittemeijer E.J. & Vogels A.B.P. (1982) Use of the Voigt function in a single-line method for the analysis of X-ray diffraction line broadening. *J. Appl. Crystallogr.* **15**, 308–314.

De Loys F. (1928) Monographie géologique de la Dent du Midi. *Matériaux Carte géol. Suisse*, **58**, 80.

Elliott D. (1970) Determination of finite strain and initial shape from deformed elliptical objects. *Geol. Soc. Am. Bull.* **81**, 2221–2236.

Flehmig W. (1973) Kristallinität und Infrarotspektroskopie natürlicher dioktaedrischer Illite. *Neues Jahrb. Mineral. Mon.* 351–361.

Flehmig W. & Langheinrich G. (1974) Beziehung zwischentektonischer Deformation und Illit-Kristallinität. *Neues Jahrb. Geol. Paläontol. Abh.* **146**, 325–326.

Frey M. (1987) *Low Temperature Metamorphism*. Blackie, Glasgow.

Frey M. & Robinson D. (1999) *Low Grade Metamorphism*. Blackwell Science, Oxford.

Gagnebin E. (1934) Notice explicative Feuille 483 St-Maurice (Feuille 8 de l'Atlas). P. 6 in: *Geologischer Atlas der Schweiz, 1:25 000*. Commision Géologique Suisse.

Gendzwill D.J. & Stauffer M.R. (1981) Analysis of triaxial ellipsoids; their shapes, plane sections, and plane projections. *J. Int. Assoc. Mathematical Geol.* **13**, 135–152.

Goy-Eggenberger D. (1998) *Faible métamorphisme de la nappe de Morcles: minéralogie et géochimie*. PhD thesis, Neuchâtel Univ. Switzerland.

Kisch H.J. (1990) Calibration of the anchizone:a critical comparison of illite 'crystallinity' scales used for definition. *J. Metam. Geol.* **8**, 31–46.

Kübler B. (1964) Les argiles, indicateurs de métamorphisme. *Rev. Inst. Franç. Pétrole* **19**, 1093–1112.

Kübler B. (1967) La cristallinité de l'illite et les zones tout à fait supérieures du métamorphisme. Pp. 105–121 in: *Etages Tectoniques, Colloque de Neuchâtel 1966* (Geology Institute Neuchâtel). La Baconnière, Neuchâtel, Switzerland.

Mayoraz R. (1995) Les brèches tertiaires du flanc inverse de la nappe de Morcles et des unités parautochthones (Bas Valais, Suisse). *Eclog. geol. Helv.* **88**, 321–345.

McCaig A.M. & Knipe R.J. (1990) Mass-transport mechanisms in deforming rocks; recognition using microstructural and microchemical criteria. *Geol.* **18**,

824−827.
Milton N.J. (1980) Determination of the strain ellipsoid from measurements on any three sections. *Tectonophysics*, **64**, T19−T27.
NCSA (1997) *Image 3.0*., ftp://ftp.ncsa.uiuc.edu/Mac/Image/, Univ. Illinois, USA.
Nyk R. (1985) Illite crystallinity in Devonian slates of the Meggen mine (Rhenisch Massif. *Neues Jahrb. Mineral. Mon.* **6**, 268−276.
Ramsay J.G. & Huber I.M. (1983) *The Techniques of Modern Structural Geology Vol. 1*. Academic Press, London.
Ramsay J.G. & Huber I.M. (1987) *The Techniques of Modern Structural Geology Vol. 2*. Academic Press, London.
Roberts B., Merriman R.J. & Pratt W. (1991) The influence of strain, lithology and stratigraphical depth on white mica (illite) crystallinity in mudrocks from the vicinity of the Corris slate belt, Wales; implications for the timing of metamorphism in the Welsh Basin. *Geol. Mag.* **128**, 633−645.
Shimamoto T. & Ikeda Y. (1976) A simple algebraic method for strain estimation from deformed ellipsoidal objects-I. Basic theory. *Tectonophysics*, **36**, 315−337.
Siddans A. (1971) *The origin of slaty cleavage*. PhD thesis, Univ. London.
Siddans A. (1983) Finite strain pattern in some Alpine nappes. *J. Struct. Geol.* **3/4**, 441−448.
Urai J.L., Means W.D. & Lister G.S. (1986) Dynamic recrystallization of minerals. Pp. 161−199 in: *Mineral and Rock deformation: Laboratory studies* (B.E. Hobbs & H.C. Heard, editors). AGU Monograph, **36**. American Geophysical Union.
Warren B.E. & Averbach B.L. (1950) The effect of cold-work distortion on X-ray patterns. *J. App. Phys.* **21**, 595−599.